https://doi.org/10.46861/bmp.32.037 PŮVODNÍ PRÁCE/ORIGINAL PAPER

Chenowethite, rare Mg-uranyl -sulphate, from the Jáchymov ore district, Krušné hory Mountains (Czech Republic) - description and Raman spectroscopy

Jiří Sejkora[1)]* and Jakub Plášil[2)]

[1)]*Department of Mineralogy and Petrology, National Museum, Cirkusová 1740, 193 00 Praha 9 - Horní Počernice; *e-mail: jiri.sejkora@nm.cz*
[2)]*Institute of Physics of the Czech Academy of Sciences, Na Slovance 1999/2, 182 00 Praha 8, Czech Republic*

Sejkora J, Plášil J (2024) Chenowethite, rare Mg-uranyl -sulphate, from the Jáchymov ore district, Krušné hory Mountains (Czech Republic) - description and Raman spectroscopy. Bull Mineral Petrolog 32(1): 37-44 ISSN 2570-7337

Abstract

We studied a rare magnesium uranyl sulphate mineral, chenowethite, from the Jáchymov ore district, Krušné hory Mountains (Czech Republic). It was confirmed from the two samples originating from the Svornost mine in Jáchymov. Chenowethite forms rich crystalline aggregates on supergene-altered rocks in association with dark yellow to orange mineral of the zippeite group and white acicular crystals of gypsum. Its randomly arranged aggregates are composed of elongated thin tabular crystals up to 100 μm in length. Chenowethite is pale or bright yellow with a pale yellow streak and fluoresces greenish yellow, weak or dull under 254 nm and 366 nm UV-radiation, respectively. Chenowethite crystals are transparent to translucent and have an intensive vitreous luster. It is very brittle, and at least one system of perfect cleavage (along {010}) was observed. The quantitative chemical analyses of chenowethite agree well with the proposed ideal composition and correspond to the following empirical formulae (on the basis of 2 U atoms *pfu*) $(Mg_{1.02}Fe_{0.03}Mn_{0.03})_{\Sigma 1.08}[(UO_2)_2(SO_4)_{2.06}(OH)_{2.04}]\cdot 11H_2O$ (sample A) and $(Mg_{0.92}Fe_{0.11}Mn_{0.04}Zn_{0.01})_{\Sigma 1.08}[(UO_2)_2(SO_4)_{1.96}(SiO_4)_{0.01}(OH)_{2.23}]\cdot 11H_2O$ (sample B). Chenowethite is orthorhombic, the space group *Cmcm*, with the unit-cell parameters refined from X-ray powder diffraction data: *a* 6.9329(8), *b* 19.0019(15), *c* 16.3298(15) Å and *V* 2151.2(3) Å^3 (sample A) and *a* 6.937(3), *b* 19.019(5), *c* 16.348(6) Å and *V* 2156.8(1.1) Å^3 (sample B). Vibrational (Raman and infrared) spectroscopy documents the presence of molecular water, uranyl and sulphate units in the crystal structure of chenowethite.

***Key words**: chenowethite, uranyl sulphate, unit-cell parameters, chemical composition, Raman spectroscopy, infrared spectroscopy, Jáchymov, Czech Republic*

Received 12. 4. 2024; accepted 17. 6. 2024

Introduction

Uranyl sulphates are common supergene alteration products formed by oxidation-hydration weathering of uraninite (Plášil 2014) associated with sulphides, such as pyrite or chalcopyrite (Finch, Murakami 1999; Krivovichev, Plášil 2013). More specifically, in old mining workings, oxidizing weathering of sulphides generates acid solutions that react with primary uraninite to form the uranyl sulphates (Fernandes et al. 1995; Brugger et al. 2003; Plášil et al. 2014).

Chenowethite, $Mg(H_2O)_6[(UO_2)_2(SO_4)_2(OH)_2]\cdot 5H_2O$, has been described recently by Kampf et al. (2022) as a new mineral from the Blue Lizard, Green Lizard and Markey mines in the White Canyon mining district, Red Canyon, San Juan County, Utah (USA). At type localities, chenowethite forms transparent pale green-yellow thin blade crystals up to 0.5 mm in length (Kampf et al. 2022). This paper aims to summarize the results of the complex mineralogical study, including Raman and infrared spectroscopy of this rare magnesium uranyl sulphate mineral on the base of finds of well crystallized samples in the Jáchymov ore district, Czech Republic.

Occurrence and specimen description

Chenowethite was found on specimens originating from the Jáchymov ore district (formerly St. Joachimsthal), Krušné hory Mountains, approximately 20 km north of Karlovy Vary, northwestern Bohemia, Czech Republic. The material we studied most probably originates from the Jan Evangelista vein at the level Daniel of the Svornost mine located in the central part of this ore district, and was collected by the mineralogist Dr. Jan Hloušek.

The Jáchymov ore district is a classic example of Ag+As+Co+Ni+Bi and U vein-type hydrothermal mineralization. The ore veins cut a complex of medium-grade metasedimentary rocks of Cambrian to Ordovician age, in a Variscan granite pluton envelope. Most of ore minerals formed during the Variscan mineralizing epoch from mesothermal fluids (Ondruš et al. 2003a,b,d). Primary and supergene mineralization in this district resulted in extraordinarily varied associations; more than 440 mineral species have been reported from there (Ondruš et al. 1997a,b and 2003c,d; Hloušek et al. 2014; Škácha et al. 2019).

Chenowethite has been found on two samples (A and B in the following text) and forms rich crystalline aggregates (Figs. 1 - 3) on supergene-altered rocks in association

Fig. 1 *Rich crystalline aggregate of chenowethite on supergene-altered rock from Jáchymov (sample A); field of view 6 mm; photo J. Sejkora.*

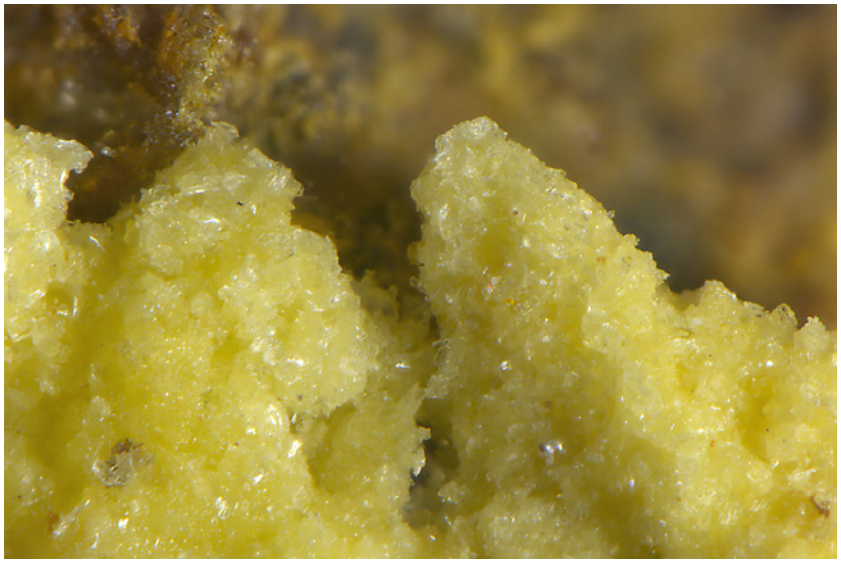

Fig. 2 *Crystalline aggregate of chenowethite formed by elongated thin tabular crystals from Jáchymov (sample A); field of view 1.2 mm; photo J. Sejkora.*

Fig. 3 *Crystalline aggregate of chenowethite formed by elongated thin tabular crystals from Jáchymov (sample B); field of view 2 mm; photo J. Sejkora.*

with dark yellow to orange mineral of zippeite group and white acicular crystals of gypsum. Its randomly arranged aggregates are composed of elongated thin tabular crystals up to 100 μm in length (Fig. 4). The mineral is pale (sample A) or bright yellow (sample B), with pale yellow streak and fluoresces greenish yellow, weak to dull under both 254 nm and 366 nm UV-radiation. Crystals are transparent to translucent and have an intensive vitreous luster. It is very brittle and at least one system of perfect cleavage (probably along {010}) was observed.

Chemical composition

Samples of chenowethite were analysed with a Cameca SX-100 electron microprobe (National Museum, Prague) operating in the wavelength-dispersive mode with an accelerating voltage of 15 kV, a specimen current of 5 nA, and a beam diameter of 10 μm. The following lines and standards were used: *K*α: albite (Na), celestine (S), chalcopyrite (Cu), Co (Co), Cr_2O_3 (Cr), diopside (Mg), fluorapatite (Ca, P), halite (Cl), hematite (Fe), LiF (F), Ni (Ni), rhodonite (Mn), sanidine (Al, Si, K), vanadinite (V), ZnO (Zn); *L*α: baryte (Ba), clinoclase (As), wulfenite (Mo), YVO_4 (Y); *L*β: celestine (Sr); and *M*α: Bi (Bi), UO_2 (U), wulfenite (Pb). Peak counting times (CT) were 20 s; CT for each background was one-half of the peak time. The raw intensities were converted to the concentrations automatically using the *PAP* (Pouchou and Pichoir 1985) matrix-correction algorithm. The contents of Al, As, Ba, Bi, Ca, Cl, Cr, F, K, Mo, Na, P, Pb, Sr, V and Y were also measured but always found to be below the detection limits (about 0.05 - 0.10 wt. %). Water content could not be analysed directly because of the minute amount of material available. The absence of carbonate and ammonium groups and the presence of H_2O were confirmed by infrared spectroscopy. A large range of experimental totals could be a result of (i) H_2O loss under vacuum in the EPMA chamber; (ii) uneven surface of samples; and (iii) small size of crystals and resulting porosity of aggregates.

Chemical composition of studied samples (Table 1) agrees very well with the ideal formula of chenowethite $Mg[(UO_2)_2(SO_4)_2(OH)_2]\cdot 11H_2O$, and published analyses of this mineral phase from type locality (Kampf et al. 2022). The cationic site is

occupied by dominant Mg with minor contents of Fe (up to 0.20 *apfu*) and Mn (up to 0.04 *apfu*) and in the case of sample B also traces of Cu, Cu, Ni and Zn. The empirical formulae of chenowethite on the basis of 2 U atoms *pfu* are $(Mg_{1.02}Fe_{0.03}Mn_{0.03})_{\Sigma 1.08}[(UO_2)_2(SO_4)_{2.06}(OH)_{2.04}]\cdot 11H_2O$ (mean of 9 analyses at sample A) and $(Mg_{0.92}Fe_{0.11}Mn_{0.04}Zn_{0.01})_{\Sigma 1.08}[(UO_2)_2(SO_4)_{1.96}(SiO_4)_{0.01}(OH)_{2.23}]\cdot 11H_2O$ (mean of 11 analyses at sample B). A partial vacancy in the Mg site and minor $(NH_4)^+$ contents described for chenowethite from the type locality (Kampf et al. 2022) were not observed in the studied samples from Jáchymov.

X-ray powder diffraction

Powder X-ray diffraction data were collected on a Bruker D8 Advance diffractometer (National Museum, Prague) with a solid-state 1D LynxEye detector using CuK_α radiation and operating at 40 kV and 40 mA. The powder pattern was collected using Bragg-Brentano geometry in the range 2.5 - 70° 2θ, in 0.01° steps with a counting time of 20 s per step. Positions and intensities of reflections were found and refined using the Pearson-VII profile-shape function with the ZDS program package (Ondruš 1993) and the unit-cell parameters were refined by the least-squares algorithm implemented by Burnham (1962). The experimental powder pattern was indexed in

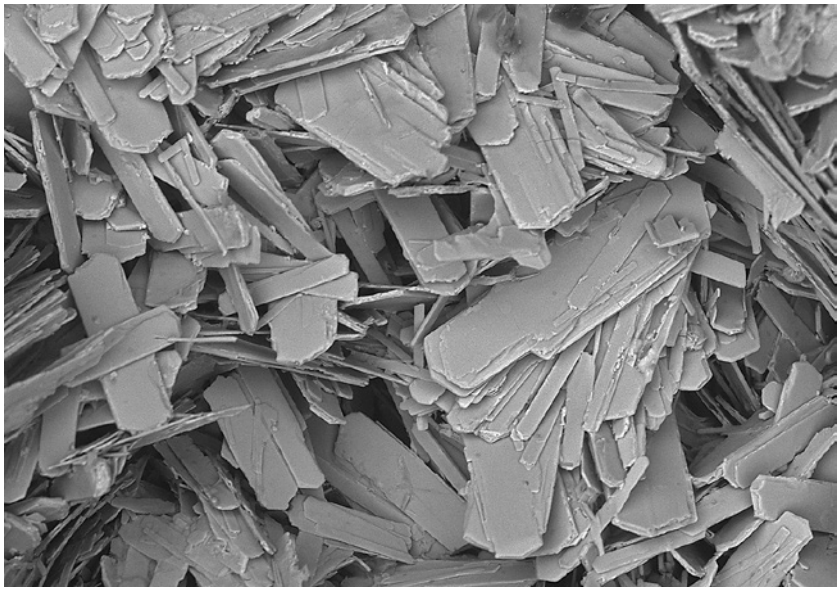

Fig. 4 *Aggregates of elongated thin tabular crystals of chenowethite from Jáchymov (sample B); field of view 250 μm; BSE photo J. Sejkora.*

Table 1 *Chemical composition of chenowethite (wt. %)*

	Jáchymov sample A		Jáchymov sample B		Red Canyon		ideal
	this paper		this paper		Kampf et al. (2022)		composition
wt.%	mean	range (n = 9)	mean	range (n = 11)	mean	range (n = 8)	
$(NH_4)_2O$					0.60	0.43 - 0.70	
FeO	0.23	0.14 - 0.31	0.81	0.36 - 1.31	0.67	0.52 - 0.94	
MgO	4.05	3.19 - 4.41	3.78	2.52 - 5.06	2.96	2.50 - 3.46	4.08
CuO			0.02	0 - 0.11			
CoO			0.03	0 - 0.09	0.35	0.30 - 0.46	
NiO			0.04	0 - 0.11	0.29	0.24 - 0.34	
MnO	0.23	0.17 - 0.30	0.27	0 - 0.70			
ZnO			0.08	0 - 0.32			
SiO_2			0.06	0 - 0.22			
SO_3	16.31	15.56 - 16.86	15.96	11.53 - 19.79	16.61	15.73 - 17.33	16.20
UO_3	56.48	53.78 - 59.73	58.26	50.52 - 66.48	59.33	58.42 - 60.07	57.86
H_2O*	21.38	20.44 - 22.40	22.22	19.18 - 25.29	22.03		21.87
total	98.68	94.63 - 102.55	101.51	87.77 - 117.69	102.84		100.00
apfu on the base U = 2							
NH_4					0.222		
Fe	0.032		0.111		0.090		
Mg	1.017		0.921		0.708		1.000
Cu			0.002				
Co			0.003		0.045		
Ni			0.004		0.037		
Mn	0.033		0.037				
Zn			0.010				
Si			0.009				
S	2.064		1.957		2.000		2.000
U	2.000		2.000		2.000		2.022
OH	2.036		2.227		1.982		2.000
H_2O	11		11		10.800		11

H_2O* was calculated based on the charge balance and ideal content of 11 water molecules *pfu*.

line with the calculated intensities values obtained from the crystal structure of chenowethite (Kampf et al. 2022), based on the Lazy Pulverix program (Yvon et al. 1977).

The peak positions in experimental X-ray powder patterns (Table 2) agree well with data published for chenowethite from type locality (Kampf et al. 2022) as well as with those calculated from the crystal structure of this mineral. Some observed differences in intensities of individual diffraction maxima are due to the preferred orientation effects. The refined unit-cell parameters, compared with published data, are given in Table 3.

Raman spectroscopy

The Raman spectra of studied samples were collected in the range 4000 - 40 cm^{-1} using a DXR dispersive Raman Spectrometer (Thermo Scientific) mounted on a confocal Olympus microscope. The Raman signal was excited by an unpolarised green 532 nm solid state, diode-pumped laser and detected by a CCD detector. The experimental parameters were: 100x objective, 10 s exposure time, 100 exposures, 50 μm pinhole spectrograph aperture and 2 mW laser power level. The spectra were repeatedly acquired from different grains to obtain a representative spectrum with the best signal-to-noise ratio. The eventual thermal damage of the measured point was excluded by visual inspection of the excited surface after measurement, by observation of possible decay of spectral features at the start of excitation and by checking for thermal downshift of Raman lines. The instrument was set up using a software-controlled calibration procedure using multiple neon emission lines (wavelength calibration), multiple polystyrene Raman bands (laser-frequency calibration), and standardized white-light sources (intensity calibration). Spectral manipulations were performed using the Omnic 9 software (Thermo Scientific).

Chenowethite, $Mg(H_2O)_6[(UO_2)_2(SO_4)_2(OH)_2]\cdot 5H_2O$, is an orthorhombic uranyl-containing mineral, the space group *Cmcm*, $Z = 4$. The crystal structure of chenowethite contains pairs of UO_7 pentagonal bipyramids that share a common edge, forming dimers. These dimers are linked by sharing corners with SO_4 groups, yielding a $[(UO_2)_2(SO_4)2(OH)_2]^{2-}$ sheets that are topologically equivalent to those in deliensite, plášilite, greenlizardite, johannite, feynmannite and meitnerite. The interlayer in the chenowethite crystal structure contains a disordered $Mg(H_2O)_6$ octahedron and three isolated H_2O groups (Kampf et al. 2022).

In general, molecular water (C_{2v} symmetry) is characterized by three fundamental ν_1 (A_1) symmetric stretching

Table 2 *X-ray powder diffraction data of chenowethite from Jáchymov*

sample A			sample B						sample A			sample B					
$I_{obs.}$	$d_{obs.}$	$d_{calc.}$	$I_{obs.}$	$d_{obs.}$	$d_{calc.}$	*h*	*k*	*l*	$I_{obs.}$	$d_{obs.}$	$d_{calc.}$	$I_{obs.}$	$d_{obs.}$	$d_{calc.}$	*h*	*k*	*l*
100.0	9.503	9.501	100	9.522	9.510	0	2	0	1.7	2.546	2.546	0.2	2.548	2.548	2	2	4
4.9	8.218	8.212	2.4	8.230	8.220	0	2	1	2.4	2.528	2.528	0.7	2.531	2.530	1	7	0
5.3	6.051	6.050	0.6	6.064	6.054	1	1	1	2.2	2.3507	2.3522	1	2.353	2.355	1	3	6
25.4	4.751	4.750	17.9	4.757	4.755	0	4	0			2.3505			2.353	0	8	1
3.3	4.675	4.676	1.3	4.687	4.680	1	3	0	0.9	2.3094	2.3092				2	4	4
8.9	4.563	4.561	4.7	4.571	4.566	0	4	1	1.5	2.2724	2.2718	0.2	2.2706	2.2731	3	1	1
1.7	4.496	4.496				1	3	1	0.9	2.1769	2.1770	0.4	2.1782	2.1791	0	8	3
1.3	4.175	4.177	0.2	4.181	4.180	1	1	3	0.4	2.1713	2.1710			2.1723	3	3	0
6.8	4.083	4.082	9.5	4.087	4.087	0	0	4	1.5	2.1492	2.1491	0.3	2.1501	2.1511	1	7	4
7.9	3.752	3.751	4	3.756	3.755	0	2	4	1.5	2.0415	2.0412	1.5	2.0425	2.0435	0	0	8
3.9	3.578	3.579	0.6	3.583	3.583	0	4	3	0.6	2.0189	2.0197	0.2	2.0214	2.0215	1	9	0
5.9	3.461	3.466	0.6	3.471	3.468	2	0	0	0.2	1.9208	1.9209	0.3	1.9219	1.9228	0	8	5
2.8	3.333	3.333	1.3	3.339	3.335	1	5	0	1.8	1.9003	1.9011	1.2	1.9015	1.9028	2	6	5
2.8	3.257	3.256	0.2	3.252	3.258	2	2	0	1.7	1.8879	1.8875	0.5	1.8893	1.8892	0	10	1
1.7	3.167	3.167	1.4	3.170	3.170	0	6	0	0.9	1.8773	1.8772	0.2	1.8762	1.8786	3	1	5
3.9	3.110	3.109	1.2	3.113	3.112	0	6	1	0.6	1.8709	1.8708			1.8727	1	3	8
2.0	3.096	3.096	1.1	3.100	3.099	0	4	4	1.1	1.8100	1.8103	0.2	1.8124	1.8120	1	9	4
2.2	3.091	3.089	1.5	3.092	3.092	0	2	5	0.6	1.7779	1.7776				3	5	4
5.0	2.920	2.919	1	2.922	2.922	1	1	5	0.4	1.7595	1.7597				3	7	0
1.3	2.800	2.800				2	4	0	0.9	1.7475	1.7479				1	1	9
0.9	2.738	2.737	0.5	2.740	2.740	0	6	3	0.6	1.6915	1.6916				1	3	9
1.3	2.677	2.678				1	3	5	0.4	1.6165	1.6159				3	7	4
3.1	2.643	2.642	0.2	2.644	2.644	2	0	4	0.7	1.5883	1.5881				1	7	8
2.4	2.582	2.582				1	5	4	0.6	1.5834	1.5835	0.5	1.5844	1.5849	0	12	0

Table 3 *Unit-cell parameters for chenowethite (for orthorhombic space group Cmcm)*

		a [Å]	*b* [Å]	*c* [Å]	*V* [Å^3]
Jáchymov A	this paper	6.9329(8)	19.0019(15)	16.3298(15)	2151.2(3)
Jáchymov B	this paper	6.937(3)	19.019(5)	16.348(6)	2156.8(1.1)
Red Canyon[1]	Kampf et al. (2022)	6.9435(6)	19.035(2)	16.3577(13)	2162.0(3)
Red Canyon[2]	Kampf et al. (2022)	6.951(2)	19.053(6)	16.372(5)	2168.19(7)

Red Canyon[1] - single crystal X-ray data; Red Canyon[2] - X-ray powder diffraction data.

OH vibrations (~3657 cm^{-1}), ν_2 (δ H_2O) (A_1) bending vibrations (~1595 cm^{-1}) and ν_3 (B_1) antisymmetric stretching OH (~3756 cm^{-1}) vibrations. All vibrations are Raman and infrared active. Their wavenumbers are influenced by the formation of hydrogen bonds. At wavenumbers lower than 1100 cm^{-1}, libration modes of water molecules may be observed (Čejka 1999; Nakamoto 2009). A free uranyl cation, $(UO_2)^{2+}$, $D_{\infty h}$ point-group symmetry, is, in general, characterized by three fundamental vibration modes: the ν_1 symmetric stretching vibration, Raman active (900 - 750 cm^{-1}), the ν_2 (δ) doubly degenerate bending vibration, infrared active (300 - 200 cm^{-1}), and the ν_3 antisymmetric stretching vibrations, infrared active (1000 - 850 cm^{-1}). The lowering of the ideal symmetry (due to crystal field and so on) may cause splitting of the ν_2 (δ) vibration and Raman and infrared activation of all three vibrations (Čejka 1999; Nakamoto 2009). A free sulphate anion, $(SO_4)^{2-}$, T_d point-group symmetry, is characterized by four fundamental modes: the ν_1 symmetric stretching vibration, Raman active (~983 cm^{-1}), the ν_2 (δ) doubly degenerate bending vibration, Raman active (~450 cm^{-1}), the ν_3 triply degenerate antisymmetric stretching vibration, Raman and infrared active, (~1105 cm^{-1}), and the ν_4 (δ) triply degenerate bending vibration, Raman and infrared active (~611 cm^{-1}). T_d symmetry lowering may cause splitting of degenerate vibrations and Raman and infrared activation of all vibrations (Čejka 1999; Nakamoto 2009)

The Raman spectra of both chenowethite samples from Jáchymov, recently studied, are close to each other and correspond to the published spectrum of chenowethite from Red Canyon (Kampf et al. 2022). The full-range Raman spectra of the studied chenowethite samples are given in Figure 5, and wavenumbers with assignments are given in Table 4; in the following text, we discuss the data for sample A. Bands of the low intensity,

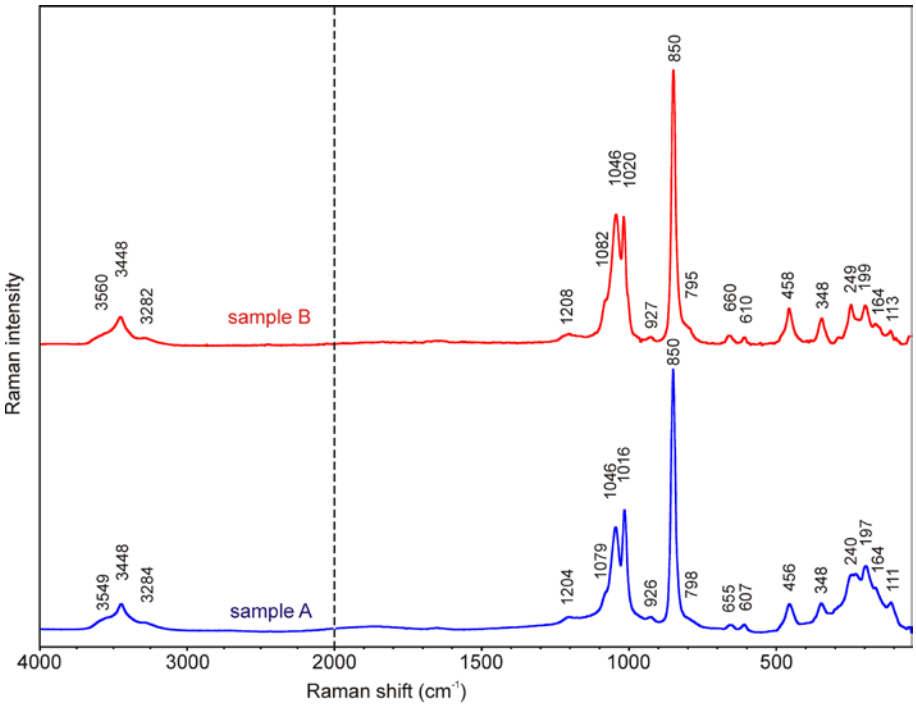

Fig. 5 *Raman spectra for chenowethite from Jáchymov (split at 2000 cm^{-1}).*

Table 4 *Tentative assignment of Raman spectra of chenowethite from Jáchymov*

sample A	*sample B*	*Red Canyon**	*tentative assignment*
[cm^{-1}]	[cm^{-1}]	[cm^{-1}]	
3549 3448 3284	3560 3448 3282	3436	ν O-H stretch of hydrogen bonded water molecules
1204	1208	1210 1176	ν_3 antisymmetric stretch of $(SO_4)^{2-}$
1079 1046 1016	1082 1046 1020	1077 1040 1015	ν_1 symmetric stretch of $(SO_4)^{2-}$
926	927	927	ν_3 antisymmetric stretch of $(UO_2)^{2+}$
850 798	850 795	846 800	ν_1 symmetric stretch of $(UO_2)^{2+}$
655 607	660 610	656 604	ν_4 bend of $(SO_4)^{2-}$
456	458	452	ν_2 bend of $(SO_4)^{2-}$
348	348	341	ν U-O_{eq}
240 197	249 199	244 196	ν_2 bend of $(UO_2)^{2+}$
164 111	164 113	160 147 109	lattice and other modes

Red Canyon* - Kampf et al. (2022).

located at 3549, 3448 and 3284 cm^{-1}, are connected with the ν OH stretching vibrations of hydrogen-bonded water molecules; according to the empirical relation between the energy of vibration and the corresponding bond length (Libowitzky 1999), O-H···O hydrogen-bond lengths vary approximately in the range from 2.73 to 3.0 Å. The broad character of Raman bands in this region and the complex nature of the interlayer part of the crystal structure, which includes several different H_2O groups, partly disordered (Kampf et al. 2022), make the unambiguous assignment of the specific hydrogen bonds impossible. A low band at 1204 cm^{-1} is assigned to the triply degenerate ν_3 $(SO_4)^{2-}$ antisymmetric stretching vibration. Medium strong bands at 1046 and 1016 cm^{-1} with a shoulder at 1079 cm^{-1} are attributed to the ν_1 $(SO_4)^{2-}$ symmetric stretching vibrations. A very weak band at 926 cm^{-1} is related to the ν_3 $(UO_2)^{2+}$ antisymmetric stretching vibrations and a very strong band at 850 cm^{-1} with a shoulder at 798 cm^{-1} is assigned to the ν_1 $(UO_2)^{2+}$ symmetric stretching vibrations. According to the empirical relationship of Bartlett and Cooney (1989), the ν_3 $(UO_2)^{2+}$ and ν_1 $(UO_2)^{2+}$, respectively, correspond to an approximate U-O bond length of 1.77 and 1.76 Å, in excellent agreement with U-O bond lengths from the X-ray data: 1.756(12) and 1.766(12) Å (Kampf et al. 2022). Two very weak bands at 655 and 607 cm^{-1} are connected with the split triply degenerate ν_4 (δ) $(SO_4)^{2-}$ bending vibrations. A band at 456 cm^{-1} is assigned to the doubly degenerate ν_2 $(SO_4)^{2-}$ bending vibrations; a weak band at 333 cm^{-1} may be associated with ν U-O_{eq} vibration (Kampf et al. 2022). Medium-intensity bands at 240 and 197 cm^{-1} are related to the ν_2 $(UO_2)^{2+}$ doubly degenerate bending vibrations; weak bands at 164 and 111 cm^{-1} may be attributed to O_{eq}-U-O_{eq} bending vibrations (Ohwada 1976), U-O_{eq}-ligand stretching modes (Bullock, Paret 1970; Ohwada 1976; Plášil et al. 2010), UO_2^{2+} translations and rotations and external lattice vibration modes (Plášil et al. 2010; Kampf et al. 2018).

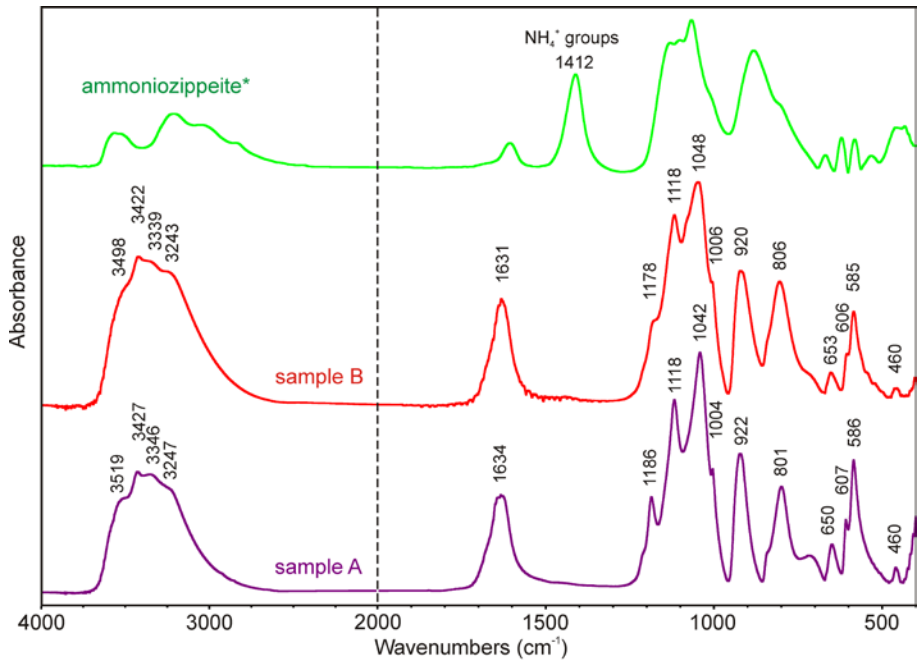

Fig. 6 *Infrared spectra for chenowethite from Jáchymov (split at 2000 cm^{-1}) compared to the spectrum of ammoniozippeite* from Jáchymov (Sejkora et al. 2023).*

Infrared spectroscopy

The infrared vibrational spectrum of chenowethite was recorded by the attenuated total reflection (ATR) method with a diamond cell on a Nicolet iS5 spectrometer. Spectra over the 4000 -

Table 5 *Tentative assignment of infrared spectra of chenowethite from Jáchymov*

sample A	*sample B*	tentative assignment
[cm^{-1}]	[cm^{-1}]	
3519	3498	ν O-H stretch of hydrogen bonded water molecules
3427	3422	
3346	3339	
3247	3243	
1634	1631	ν_2 bend of hydrogen bonded water molecules
1186	1178	ν_3 antisymmetric stretch of $(SO_4)^{2-}$
1118	1118	
1042	1048	ν_1 symmetric stretch of $(SO_4)^{2-}$
1004	1006	
922	920	ν_3 antisymmetric stretch of $(UO_2)^{2+}$
801	806	ν_1 symmetric stretch of $(UO_2)^{2+}$ and/or libration mode of H_2O
650	653	ν_4 bend of $(SO_4)^{2-}$
607	606	
586	585	ν_4 bend of $(SO_4)^{2-}$ and/or libration mode of H_2O
460	460	ν_2 bend of $(SO_4)^{2-}$

400 cm^{-1} range were obtained by the co-addition of 64 scans with a resolution of 4 cm^{-1} and a mirror velocity of 0.4747 cm/s. Spectra were co-added to improve the signal-to-noise ratio.

The IR spectrum of chenowethite has not been published yet. The full-range spectra of samples from Jáchymov are given in Figure 6, and the tentative assignment is in Table 5; both spectra are close to each other and in the following text, we discuss the data for sample A. The experimental spectra confirm the absence of NH_4^+ groups (characteristic band about 1400 cm^{-1}) in the studied samples (Fig. 6). Strong and broad infrared bands at 3519, 3427, 3346 and 3247 cm^{-1} are assigned to the ν O-H stretching vibration of hydrogen-bonded water molecules, according to Libowitzky (1999) correlation function, O-H···O hydrogen bond lengths vary approximately from 2.9 to 2.71 Å. A medium-strong infrared band at 1634 cm^{-1} is attributed to the ν_2 H_2O bending vibration of water molecules. Infrared bands at 1186 and 1118 cm^{-1} are assigned to the split triply degenerate ν_3 $(SO_4)^{2-}$ antisymmetric stretching vibrations, and those at 1042 and 1004 cm^{-1} to the ν_1 $(SO_4)^{2-}$ symmetric stretching vibrations. A strong infrared band at 926 cm^{-1} is attributed to ν_3 $(UO_2)^{2+}$ antisymmetric stretching vibrations, calculated uranyl U-O bond length (Bartlett, Cooney 1989) 1.77 Å is comparable with bond lengths from the X-ray data (Kampf et al. 2022). The medium-strong infrared band at 801 cm^{-1} may be connected with ν_1 $(UO_2)^{2+}$ symmetric stretching vibration and/or libration mode of H_2O molecules (Kampf et al. 2018); the later assignment is more probable, the calculated bond length (Bartlett, Cooney 1989) 1.81 Å does not correspond to bond length from X-ray data very well. Weak and medium strong bands at 650, 607 and 586 cm^{-1} are attributed to the split triply degenerate ν_4 $(SO_4)^{2-}$ bending vibrations, and the band at 586 cm^{-1} may also be connected with the libration mode of water molecules (Sejkora et al. 2023). A weak infrared band at 460 cm^{-1} is related to the doubly degenerate ν_2 $(SO_4)^{2-}$ bending vibration.

Conclusion

Very rare Mg uranyl sulphate, chenowethite, was determined from specimens from the Jáchymov ore district (Czech Republic) by X-ray powder diffraction and electron microprobe analyses. The molecular structure of this well-defined sample can be better constrained using vibrational spectroscopy. Raman and infrared spectroscopy confirmed the presence of molecular water, uranyl and sulphate units in its crystal structure.

Acknowledgements

The study was financially supported by the Ministry of Culture of the Czech Republic (long-term project DKRVO 2024-2028/1.II.a; National Museum, 00023272). J. P. acknowledges the support by the project CzechNanoLab by MEYS CR (LM2018110).

References

Bartlett JR, Cooney RP (1989) On the determination of uranium-oxygen bond lengths in dioxouranium(VI) compounds by Raman spectroscopy. J Mol Struct 193: 295-300

Brugger J, Burns PC, Meisser N (2003) Contribution to the mineralogy of acid drainage of uranium minerals: marécottite and the zippeite group. Am Mineral 88: 676-685

Bullock H, Parret FW (1970) The low frequency infrared and Raman spectroscopic studies of some uranyl complexes: the deformation frequency of the uranyl ion. Can J Chem 48: 3095-3097

Burnham Ch W (1962) Lattice constant refinement. Carnegie Inst Washington Year Book 61: 132-135

Čejka J (1999) Infrared spectroscopy and thermal analysis of the uranyl minerals. Rev Mineral 38: 521-622

Fernandes HM, Veiga LHS, Franklin MR, Prado VCS, Taddei JF (1995) Environmental impact assessment of uranium mining and milling facilities; a study case at the Poços de Caldas uranium mining and milling site, Brazil. J Geochem Explor 52(1-2): 161-173

Finch RJ, Murakami T (1999) Systematics and paragenesis of uranium minerals. Rev Mineral 38: 91-180

Hloušek J, Plášil J, Sejkora J, Škácha P (2014) News and new minerals from Jáchymov, Czech Republic (2003 - 2014). Bull mineral-petrolog Odd Nár Muz (Praha) 22: 155-181

Kampf AR, Plášil J, Olds TA, Nash BP, Marty J (2018) Ammoniozippeite, a new uranyl sulfate mineral from the Blue Lizard Mine, San Juan County, Utah, and the Burro Mine, San Miguel County, Colorado, USA. Can Mineral 56: 235-245

Kampf AR, Plášil J, Olds TA, Ma C, Marty J (2022) Chenowethite, $Mg(H_2O)_6[(UO_2)_2(SO_4)_2(OH)_2]\cdot 5H_2O$, a new mineral with uranyl-sulfate sheets from Red Canyon, Utah, USA. Minerals, 12(12): 1594

Krivovichev SV, Plášil J (2013) Mineralogy and crystallography of uranium. In: Burns PC, Sigmon GE (eds) Uranium: From Cradle to Grave. Mineralogical Association of Canada Short Courses 43: 15-119

Libowitzky E (1999) Correlation of O-H stretching frequencies and O-H···O hydrogen bond lengths in minerals. Monat Chem 130: 1047-1059

Nakamoto K (2009) Infrared and Raman spectra of inorganic and coordination compounds Part A: Theory and applications in inorganic chemistry. John Wiley and Sons Inc. Hoboken, New Jersey

Ohwada K (1976) Infrared spectroscopic studies of some uranyl nitrate complexes. J Coord Chem 6: 75-80

Ondruš P (1993) ZDS - A computer program for analysis of X-ray powder diffraction patterns. Materials Science Forum, 133-136, 297-300, EPDIC-2. Enchede.

Ondruš P, Veselovský F, Hloušek J, Skála R, Frýda J, Čejka J, Gabašová A (1997a) Secondary minerals of the Jáchymov (Joachimsthal) ore district. J Czech Geol Soc 42: 3-76

Ondruš P, Veselovský F, Skála R, Císařová I, Hloušek J, Frýda J, Vavřín I, Čejka J, Gabašová A (1997b) New naturally occurring phases of secondary origin from Jáchymov (Joachimsthal). J Czech Geol Soc 42: 77-107

Ondruš P, Veselovský F, Gabašová A, Drábek M, Dobeš P, Malý K, Hloušek J, Sejkora J (2003a) Ore-forming processes and mineral parageneses of the Jáchymov ore district. J Czech Geol Soc 48: 157-192

Ondruš P, Veselovský F, Gabašová A, Hloušek J, Šrein V (2003b) Geology and hydrothermal vein system of the Jáchymov (Joachimsthal) ore district. J. Czech Geol. Soc. 48: 3-18

Ondruš P, Veselovský F, Gabašová A, Hloušek J, Šrein V (2003c) Supplement to secondary and rock-forming minerals of the Jáchymov ore district. J Czech Geol Soc 48: 149-155

Ondruš P, Veselovský F, Gabašová A, Hloušek J, Šrein V, Vavřín I, Skála R, Sejkora J, Drábek M (2003d) Primary minerals of the Jáchymov ore district. J Czech Geol Soc 48: 19-147

Plášil J (2014) Oxidation-hydration weathering of uraninite: the current state-of-knowledge. J Geosci 59: 99-114

Plášil J, Buixaderas E, Čejka J, Sejkora J, Jehlička J, Novák M (2010) Raman spectroscopic study of the uranyl sulphate mineral zippeite: low wavenumber and U-O stretching regions. Anal Bioanal Chem 397: 2703-2715

Plášil J, Sejkora J, Škoda R, Škácha P (2014) The recent weathering of uraninite from the Červená vein, Jáchymov (Czech Republic): a fingerprint of the primary mineralization geochemistry onto the alteration association. J Geosci 59: 223-253

Pouchou J, Pichoir F (1985) „PAP" (φρz) procedure for improved quantitative microanalysis. In: Armstrong JT (ed): Microbeam Analysis: 104-106. San Francisco Press. San Francisco

Sejkora J, Dolníček Z, Plášil J (2023) Ammoniozippeite from the Jáchymov ore district, Krušné hory Mountains (Czech Republic) - description and Raman spectroscopy. Bull Mineral Petrolog 31(1): 1-9

Škácha P, Plášil J, Horák V (2019) Jáchymov: mineralogická perla Krušnohoří. Academia, Praha 682 pp.

Yvon K, Jeitschko W, Parthé E (1977) Lazy Pulverix, a computer program for calculation X-ray and neutron diffraction powder patterns. J Appl Cryst 10: 73-74